International Journal of Fatigue 146 (2021) 106143

Contents lists available at ScienceDirect

International Journal of Fatigue

journal homepage: www.elsevier.com/locate/ijfatigue

Tension-tension fatigue behavior of hybrid glass/carbon and carbon/carbon composites

Filipe Ribeiro [a], José Sena-Cruz [b], Anastasios P. Vassilopoulos [c,*]

[a] Instituto de Soldadura e Qualidade (ISQ), R&D and Innovation, 2740-120 Porto Salvo, Portugal
[b] ISISE/IB-S, Department of Civil Engineering, University of Minho, 4800-058 Guimarães, Portugal
[c] Composite Construction Laboratory (CCLab), Ecole Polytechnique Fédérale de Lausanne (EPFL), 1015 Lausanne, Switzerland

ARTICLE INFO

Keywords:
Fatigue
Composites
Hybrid
Interlayer
Delamination growth

ABSTRACT

This work investigates the quasi-static, low-cycle and fatigue behavior of hybrid glass/ultra-high modulus carbon (GC) and low modulus/ /high modulus carbon (CC) fiber composites. These pseudo-ductile unidirectional interlayer hybrids are a new type of composites whose potential is not yet fully understood, particularly under cyclic/fatigue loading. Different test methods (digital image correlation, video extensometer and thermal camera) were used to record the evolution of the strain, damage and temperature during loading. The results of quasi-static loading shown pseudo-ductile responses with multiple fractures for all the series. The CC specimens exhibited higher initial elastic modulus, 'yield' stress and strength, while the GC specimens showed the highest pseudo-ductile strain. Much higher capacity of CC to resist to fatigue loading was observed. In the GC specimens significant damage was accumulated during fatigue loading, when the damage evolution of multiple fractures in different layers developed to delamination between the glass and carbon layers.

1. Introduction

The concept of hybrid, or mixed fiber composite, has been introduced as a natural extension of the composites' principle [1], a couple of decades after the introduction of composite materials in several engineering applications, back in the 1950s [2]. The study of hybrid composites was essentially motivated in the scope of the aerospace and automotive industries [3–5]. Hybrids were produced, attempting to reduce the cost of composites with expensive reinforcements by incorporating a proportion of cheaper, low-quality fibers without significantly reducing the properties of the initial composite. Alternatively, hybrids were produced to improve the properties of a composite by judiciously placing high quality fibers, without affecting significantly the cost [1]. The benefit from such attempts is that the material can achieve superior properties and can satisfy design requirements that could not be satisfied without the hybridization. A typical example of this can be found in the wind turbine rotor blades industry where hybrid carbon/glass technology is used to allow the production of long blades by keeping the weight and the cost in reasonable levels. Carbon fibers can be placed locally to increase the stiffness for a given blade weight, or reduce the weight for a given stiffness [6]. Hybrid composites can be produced by several different techniques depending on the way the constituent materials are mixed: (i) interlayer hybrids where layers of the two (or more) reinforcements are stacked; (ii) intralayer hybrids in which tows of the two (or more) constituent types of fibers are mixed in the same layer; (iii) intimately mixed (intermingled) hybrids where the constituent fibers are mixed as randomly as possible so that no concentrations of either type are present in the material; (iv) selective placement in which reinforcements are placed where additional strength is needed, over the base reinforcing laminate layer [7,8]. Hybridization allows utilization of the special properties of each fiber species e.g. the natural toughness of Kevlar fibers to improve the relative brittleness of carbon fibers, or the high stiffness of carbon fibers to improve the lower corresponding properties of glass and Kevlar fibers. The mix of fibers in the same matrix promotes synergies between the reinforcing materials and, usually, reduces their disadvantages [3].

The first types of hybrid composites, introduced in the 1970s, were mixtures of glass/carbon and Kevlar/carbon fibers [1,4,7,9–13]. In the following years, a certain amount of different fiber types was used to create hybrid composite materials for different aims and applications. Glass-and poly (vinyl alcohol) woven fabrics [8], polypropylene fibers mixed with glass fibers [13,14], high performance polyethylene fibers mixed with carbon fibers to create intermingled tow hybrids [15], basalt with carbon interlayer hybrids [16], unidirectional glass mixed with

* Corresponding author.
E-mail address: anastasios.vassilopoulos@epfl.ch (A.P. Vassilopoulos).

https://doi.org/10.1016/j.ijfatigue.2021.106143
Received 9 October 2020; Received in revised form 3 January 2021; Accepted 4 January 2021
Available online 7 January 2021

random glass fibers [17], high/low carbon interlayer hybrids [10], kenaf and glass hybrid bio-composites [18,19], jute and glass interplay hybrids [20], and interlayer hemp/glass mat fibers [21], were used by different research groups.

In the interlayer hybrids (focus of the present paper), it has been proven that, in some cases, an optimized gradual tensile failure process can be achieved, thus avoiding catastrophic failure. This means that, even though fiber composites are usually quasi-brittle materials, they can show pseudo-ductility when they are hybridized in an effective way [8,22,23]. This is due to the load transfer between low-strain (LS) and high-strain (HS) layers, fragmentation of the LS layers (a damage process where multiple fractures take place at LS material), followed by the stable delamination of the LS layers from the HS layers. The term 'pseudo-ductility' is used to describe the potential of achieving a flat-topped stress–strain curve of monotonic tensile tests up to the failure of some unidirectional hybrid FRP composites [22].

Furthermore, it has been observed that hybridization increases the apparent strain at LS fibers' failure [11]. This has been called in the literature the "hybrid effect". More precisely, the hybrid effect is defined as the ratio between the absolute variation of the strain at the failure of LS material (measured on UD non-hybrid and UD hybrid composites) to the strain at the failure of LS material (measured on non-hybrid composites). This effect has been one of the most commonly reported synergies of hybrid FRP composites. Although in some works the same has been defined as the deviation of different tensile mechanical properties from the rule of mixtures, today it is unanimously understood as the increase of the apparent strain at the failure of LS material.

Most of the applications using hybrid composites are facing a high number of fatigue cycles during their operational lifetime, with most of them failing due to fatigue or fatigue related phenomena [2,6]. Fatigue of hybrid composites has been investigated since their appearance in the early 1970s. First fatigue investigations, e.g. [1,7,9,15,24] attempted to investigate whether hybrid composites fatigue behavior was better than a linear mix of the constituent materials' fatigue behavior. It was shown in [25] that a (glass/carbon) hybrid material exhibit a lower S-N slope than the slopes of the pure glass and pure carbon composites for a range of fatigue load levels. Unidirectional hybrid composites made of high-performance polyethylene (HP-PE) and carbon fiber intermingled tow hybrids with a high degree of dispersion shown also a flatter S-N curve when compared to the pure carbon composites when they were fatigued between 50% and 90% of their respective static tensile strength. Modeling of the fatigue damage mechanisms in glass/carbon hybrid composites performed in [26] shown an improvement in the fatigue lifetime of hybrid composites compared to pure glass fiber composites. This improvement was attributed to the delay of crack propagation when moving from the lower strain carbon fibers to the higher strain glass fibers. According to this modeling work, increase fiber dispersion could improve the hybrid's damage resistance.

The role of fiber mixing on the fatigue behavior was investigated and it was proved to be significant [26], while it was suggested that the interlayer hybrids show the best fatigue behavior among all types of hybrid composites. The type of fibers used for the hybridization and the percentage of each type was found to affect significantly the fatigue behavior of the hybrid composites. For example, better fatigue behavior was observed in [16] for a basalt/carbon hybrid compared to a glass /carbon one. This difference was attributed to the roughness of basalt fibers which contributed to mechanical interlocking between the basalt and carbon layers thus promoting sufficient bonding between them, thereby delaying the delamination propagation.

The above-mentioned works on the fatigue behavior of unidirectional hybrid composites, agree that there is a benefit in fatigue if using fiber types with different strains to failure. The less stiff fibers prevent further rapid crack extension from the stiffer fibers and this leads to slower fatigue damage propagation and enhances fatigue life. Furthermore, the tensile fatigue resistance of hybrid composites can be improved by increasing the dispersion between the reinforced fibers and by increasing the adhesion between the low and high modulus fibers by surface treatment.

However, the fatigue response of hybrid composite systems was not extensively investigated yet, as several specific topics have been overlooked in the past. The evolution of the fatigue stiffness of composites, adhesively bonded composite joints, and structural adhesives, and that of the hysteresis loop area, have attracted the attention of several researches in the past, e.g., [27–31], although received much less attention for hybrids [6]. The same holds true for the investigation of the fatigue failure modes. Failure of composite materials is a gradual process involving different damage mechanisms that can interact with each other [32]. This damage development becomes more complicated for hybrid composites [6]. In addition, the fatigue behavior of pseudo-ductile hybrid composites has not been sufficiently explored yet, although first reports, e.g., [33] shown that catastrophic fatigue failure can be avoided by hybridization.

Ribeiro *et al.* [22,34–36] have developed an innovative hybrid composite system for confining concrete columns. These works included (i) the development of the hybrid material and (ii) its application to concrete columns under quasi-static loading and, (iii) the investigation of the fabric thickness effect on the mechanical properties. The present work details the characterization of unidirectional (UD) interlayer carbon/glass hybrid composites for civil engineering applications under quasi-static, low-cycle and fatigue loading, in order to investigate the potential of this material system to develop pseudo-ductile behavior under repeated loading conditions.

2. Pseudo-ductile behavior

Achieving pseudo-ductility can help composite materials to maintain functionality even when they are overloaded, improving the safety of composite structures. To obtain pseudo-ductility careful design of the hybrid configuration should be performed. If configuration is not correctly designed, the hybrid composite may not only break suddenly, but also shows a lower strength than the individual constituents.

Czél and Wisnom [23] showed that laminates with the same carbon/glass proportion may have different tensile responses. For example, a UD sandwich hybrid with one E-Glass layer on each side and two Carbon layer in the middle, [1 E-Glass /2 carbon /1 E-Glass], fails straightaway after the first crack in the carbon layer but the final failure strain of [2 E-Glass /4 carbon /2 E-Glass] layup, with exactly the same carbon/glass proportion, is almost double, because of their difference in delamination propagation. It has been found that initiation and propagation of hybrid composites' damage, including pseudo-ductility, depend primarily on the strength, stiffness, volume fractions of the reinforcing materials, ply thickness, stacking sequence, and toughness of mode II fracture of the interface between the reinforcing materials. Czél *et al.* [4] showed that the mode II energy release rate can be determined by the elastic properties and the thicknesses of the reinforcing material layers in the hybrid composite. Nevertheless, it is extremely difficult to define one optimal hybrid configuration. The optimal configuration depends on the property that one aims at maximizing, e.g., the hybrid effect, the 'yield' stress, the pseudo-ductile strain, the strength, the elastic modulus, or the cost, etc.

In a unidirectional hybrid FRP composite submitted to uniaxial tension, the first damage mode is the failure of the LS fibers. However, the subsequent damage modes depend on the properties and configuration of the composite reinforcing materials [37]. Four different damage modes may occur after LS fibers failure [38]: (i) premature HS failure, (ii) unstable delamination, (iii) LS layer fragmentation, and (iv) LS fragmentation and stable delamination. The behavior is called pseudo-ductile when the last one occurs.

Fig. 1 shows the schematic stress–strain pseudo-ductile curve. The 'yield' stress is defined as the stress at the point that response deviates from the initial linear elastic line, i.e., equal to the stress under which the LS fibers start failing (σ@LF). In the present work, σ@LF and the

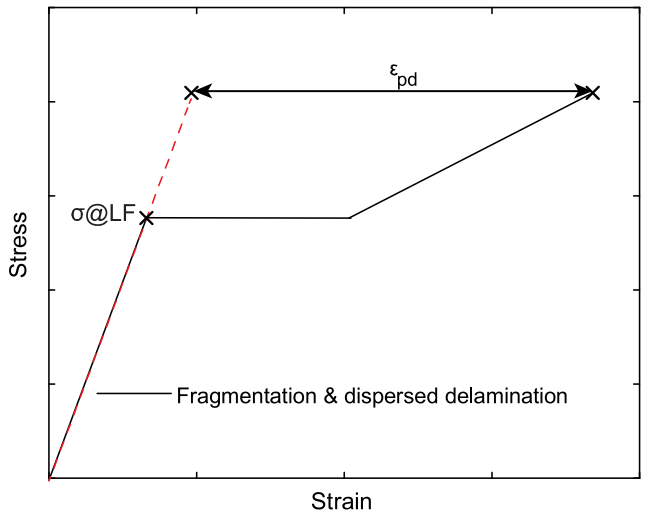

Fig. 1. Illustration of nonlinear quasi-static pseudo-ductile behavior and definition of 'yield' stress and pseudo-ductile strain.

corresponding strain at the failure of LS fibers is assumed as the first load drop because nonlinear stress–strain response before this point is not obvious. The pseudo-yield strain (ε_{pd}) is the strain level at which the tensile response deviates significantly from the initial linear elastic behavior and is defined as the extra strain between the final failure strain and the strain on the extrapolated initial slope line at the failure stress of the stress–strain diagram. The hybrid effect is defined as the enhancement in strain compared to the non-hybrid results.

3. Experimental program

3.1. Materials and test combinations

Three different dry unidirectional fabrics were used: (i) UD ultra high modulus carbon (S&P C-Sheet 640), (ii) high strength carbon (S&P C-Sheet 240), and (iii) E-glass (S&P G-sheet E 90/10). For the sake of simplicity, UD fabrics 'S&P C-Sheet 640', 'S&P C-Sheet 240' and 'S&P G-sheet E 90/10' were named as 'CHM', 'CLM' and 'G', respectively. A solvent-free, transparent 2-component epoxy resin with a formulated amine hardener (S&P Resin Epoxy 55 HP) was used for impregnating the fabrics. These materials are typically used in Civil Engineering applications.

The density, areal mass, and the fabric fiber layer thickness (ratio between areal mass density and volumetric mass density), as well as the basic tensile properties of the mentioned reinforcing materials and their coefficient of variation (COV) are presented in Table 1. In a previous work of the authors [36], single fiber properties were derived from single fibers randomly taken from dry fabrics and tested according to the ASTM D3379. The results are given here as well in order to show the diversity of modulus between the selected reinforcing materials.

The epoxy resin has been characterized in [39], by performing monotonic experiments following ISO 527–2 [40]. The specimens were cured during 7 days at 20 °C and then post-cured at 60 °C for 24 h. They were tested 26 days after mixing, under 20 °C and 50% of relative humidity. The material properties are also given in Table 1.

The glass transition temperature (T_g) of the epoxy resin was measured by a dynamic mechanical analysis (DMA). DMA experiments were performed using a TA Instruments DSC Q800 system under constant displacement of 15 μm at a frequency of 1 Hz using a single-cantilever configuration. Two specimens with geometry of 35 × 10 × 3 [mm] were tested. A heating rate of 2 °C/min was selected to run DMA scans between −20 °C and +120 °C, with a 10 min isothermal period in both extreme temperature values, according to ASTM D7028-07. The T_g, 59.5 °C (COV: 0.7%) was defined as the onset value of the storage modulus decay obtained from the intersection of the two tangent lines of the storage modulus curve, one tangent to the upper plateau and the other tangent to the linear decreasing segment at the glass transition region, as shown in Fig. 2.

Two hybrid laminates were manufactured, one combining glass and ultra-high modulus carbon fibers (GC) (with the best pseudo-ductile strain), and a second one combining high strength and ultra-high modulus carbon fibers (CC) (with the best 'yield' strain). Each reinforcing material was labelled according to the strain to failure. Within the same combination the reinforcing material with the lowest strain at failure is named as 'low-strain' (LS) and the one with the highest strain at failure is named as 'high-strain' (HS) material. Table 2 presents the configuration of the studied hybrid composites. These combinations were selected based on the experience of the authors (see [22,34,36]) in order to maximize the pseudo-ductile behavior of the resulted configurations, i.e., the combination with the best 'yield' stress and pseudo-ductile strain. Fiber volume fraction of the laminates, based on the fiber areal mass of the reinforcing materials and the thickness of the

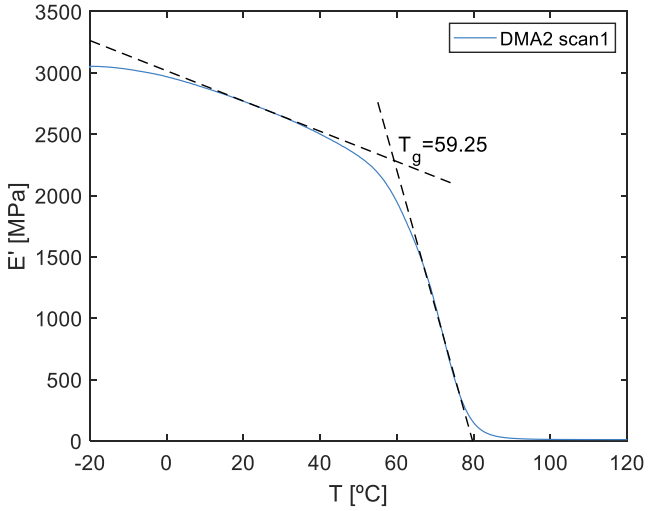

Fig. 2. Example of evolution of the storage modulus with the temperature.

Table 1
Properties of the dry fabrics and tensile properties of fibers.

Material ID	Properties of the dry fabric			Properties of the fibers (tested according to ASTM D3379)				
	Density [g/cm^3]	Areal mass [g/m^2]	Fiber layer thickness [mm/layer]	N. of samples	Fiber diameter [μm] (COV [%])	Elastic modulus [GPa] (COV [%])	Tensile strength [MPa] (COV [%])	Strain at the failure [%] (COV [%])
E-glass (G)	2.60	400	0.154	50	14.98 (16.25)	76.9 (28.0)	2662.1 (33.9)	3.72 (20.45)
HS carbon (CLM)	1.79	400	0.223	36	7.88 (5.15)	214.0 (43.4)	3920. 7 (39.4)	1.38 (17.37)
UHM carbon (CHM)	2.10	400	0.190	26	11.03 (6.66)	558.1 (24.7)	2934.2 (19.2)	0.53 (18.99)
Epoxy resin	1.15	–	–	6	–	3.5 (10.9%)	67.2 (3.2%)	3.84 (5.39%)

Table 2
Studied combinations.

Series ID	Material combination	Layer ratio (LS/HS fibers)* [%]	Fiber volume fraction** [%]	Manufacturing method	Stacking sequence
GC	2G/1CHM/2G	20/80	34.84% (CoV: 3.20%)	Hand lay-up	■■□■■
CC	1CLM/1CHM/1CLM	33/66	31.81% (CoV: 2.00%)	Hand lay-up	■□■

Notes: ■ – High strain (HS) fibers layer; □ – Low strain (LS) fibers layer; * ratio computed according the applied number of layers of each material; ** fiber volume fraction was computed considering the fiber areal mass of reinforcing materials and mean thickness of hybrid composites.

hybrid composites is also given in Table 2. The void analysis was not performed in the scope of this work. In retrofitting of existing civil structures hand lay-up is used. In this type of applications is difficult to accurately control the amount of applied resin.

3.2. Specimen's fabrication and test set-up

Hybrid composite specimens were prepared by hand layup. Prior to the manufacturing, dry fabrics were cut in rectangular pieces (400 mm × 300 mm) in order to produce composite laminates with the desired fiber architectures.

The lamination was done in a preparation room with temperature T = 21 ± 3 °C and relative humidity RH = 40 ± 10%. The epoxy resin was prepared and subjected to vacuum (1 bar pressure), for degassing during 15 min prior to the impregnation. The following fabrication protocol was followed to produce the laminates:

(i) saturation of the first fabric layer with epoxy resin (both sides with hand lay-up) and placement on a flat base, adjusting it manually;
(ii) application of pressure with a metallic roller weighting 5 kg, in order to remove both the excess of epoxy resin and the remaining air bubbles, and also to stretch and align the fibers in each fabric;
(iii) repeat the previous steps for subsequent layers positioned according to the lamination plan in order to produce the desired laminates of Table 2;
(iv) after positioning of all layers, final application of pressure by the same metallic roller to remove the excess of resin and air bubbles;
(v) curing of all laminates at room temperature for 1 day and then post-curing at 60 °C degrees for 1 h (no vacuum chamber was used).

Four laminate plates per combination were manufactured. Rectangular hybrid composite specimens were then cut from each laminate using a water jet. The geometry of the hybrid composite specimens followed the ISO 527–5 [41]. Specimens' nominal dimensions were 250/150/15 [mm] (length/free length/width). The actual cross sectional area dimensions of each specimen were measured by taking three values of thickness along the specimen free length prior to testing. GC specimens presented a thickness of 2.32 mm (COV = 4.2%) and CC specimens 2.04 mm (COV = 4.5%). Aluminum tabs of 50 × 15 × 3 [mm] were glued with cyanoacrylate glue at each end of the specimen to minimize gripping effects. All experiments were carried out on an Instron 8800 hydraulic universal testing rig of 100 kN capacity with accuracy of ±0.01 kN in an air-conditioned room (T = 22 ± 3 °C, RH = 40 ± 10%), please see Fig. 3.

Three different types of experiments were carried out, as described in the following section: (i) quasi-static, (ii) low-cycle and (iii) fatigue. The test matrix is given in Table 3.

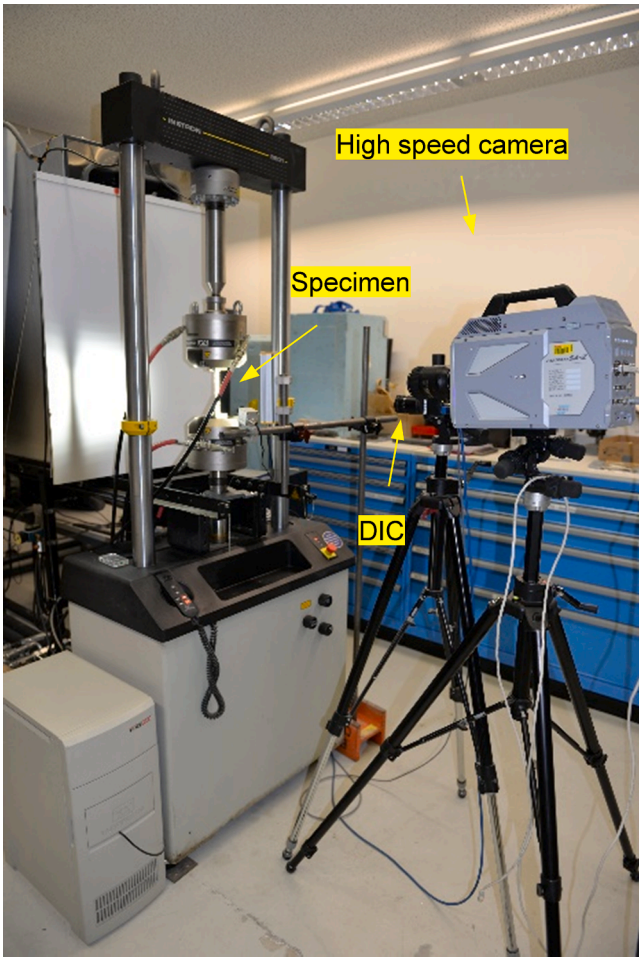

Fig. 3. Overview of the test apparatus.

3.2.1. Quasi-static experiments

For quasi-static experiments, a rate of 1 mm/min up to failure was used. The variation of the longitudinal strains was measured by a high-resolution video-extensometer (VE) or a 2D digital image correlation (DIC) system. Post processing of the results was performed by means of the commercial software GOM correlate, when it was needed to obtain a full field surface strain measurement. For both, the video extensometer and the DIC systems, a camera Point Grey - Grasshopper3 with a resolution of 2.2 Mpixels and Fujinon HF35SA-1 35 mm F/1.4 lens) was used. A frequency of acquisition of 2 images/s was adopted. Four specimens were tested per series.

3.2.2. Low-cycle experiments

Low-cycle experiments were performed under displacement control in the loading/reloading phases with a rate of 1 mm/min. Force control with a rate of 10 kN/min was adopted during the unloading phases down to a minimum tensile force of 0.5 kN. A step displacement increment of 0.25 mm, measured by the internal transducer of the testing

Table 3
Test matrix showing the examined configurations and the number of specimens.

Loading type	Configuation: 2G/1CHM/2G Series ID: GC	Configuation: 1CLM/1CHM/1CLM Series ID: CC
Quasi-static	4	4
Low-cycle	4	4
Fatigue	15	2

equipment, was adopted between loading/reloading phases. Strains were measured using the same VE and/or 2D DIC systems used for the quasi-static experiments. The stiffness was computed through linear regression, considering all the points of loading components of cycles. Four specimens were tested per series.

3.2.3. Fatigue experiments

Fatigue experiments were conducted for the GC hybrid laminates under load control by applying a sinusoidal load at a frequency of 5 Hz and the stress ratio ($R = \sigma_{min}/\sigma_{max}$) of 0.1. CC combination proved to be insensitive to fatigue tests, since during preliminary experiments the specimens were exceeding 5×10^6 cycles without any obvious damage independent of the stress level. As it is known, carbon fiber composites are relatively insensitive to tension fatigue damage even at very high stress levels [42], this is particularly the case for unidirectional composites loaded in the fiber direction. Therefore, this material configuration was not further investigated in fatigue since it was not expected that the CC specimens would show any pseudo-ductile behavior in fatigue. Loading for the fatigue experiments was applied on the specimens by a ramp up to the maximum load (F_{max}) and unloading until reaching the mean value of the cyclic load at a rate of 5 kN/min, followed by the sinusoidal constant amplitude fatigue loading. Five fatigue load levels were selected between 10 and 16 kN in order to explore different stages of the pseudo-ductile curve obtained from the quasi-static tests. As mentioned in the introduction, the fatigue loading was not intending at deriving a complete S-N curve of the material up to numbers of cycles similar to those seen during its operational lifetime. In contrast to that, relatively high cyclic stress levels were selected to explore different stages of the pseudo-ductile curve obtained from the quasi-static tests: (i) three load levels at fragmentation phase (10, 12 and 13.5 kN) and (ii) two after the saturation of specimen (15 and 16 kN). During the fragmentation phase several cracks are formed, conducting to a different type of damage progression that is observed when saturation (more stable damage progression) takes place. For this reason, more loading levels were adopted during the fragmentation phase. The surface temperature was continuously monitored by using an infrared-thermal camera (thermoIMAGER TIM), with 0.1 °C resolution to validate the selected parameters. Strains were measured by using the VE. The stiffness was computed through linear regression, considering all the points of a cyclic (unloading/reloading components). The slope of each stress–strain hysteresis loop corresponds to the fatigue stiffness [38,39].

The specimens were labelled according to the series and the maximum applied load level, followed by a serial number indicating the specimen internal code. For example, the specimen GC-F-165-813 was produced with glass and carbon (GC). It was subjected to fatigue loading (F), at 16.5 kN maximum load. The number 813 indicates that it was specimen number 13, obtained from the laminate plate number 8. All valid experimental results from the fatigue loading program are presented in Table 4. Specimens that failed during the first cycles, as well as the CC specimens that were run out were excluded.

4. Experimental results and discussion

4.1. Quasi-static experiments

Fig. 4 shows the stress–strain curves of the two examined specimen configurations. A stable pseudo-ductile response with multiple fractures was observed for both configurations, showing an initial linear behavior, followed by a slightly rising plateau and a second rising, almost, linear branch.

Comparison of the results of both material systems shows that the CC combination had the highest elastic modulus, 'yield' stress and corresponding strain and the highest strength. On the other hand, the highest values of strain at failure were achieved by the GC combination.

The mean values of the tensile properties and their coefficient of variation (COV) are presented in Table 5, for each series. The obtained results are in agreement with previous work of the authors [22,34,36]. Looking at the Table 4, it can be said that the results present small spread between them. COV varied between 6.61% and 9.06%, for the analyzed properties of GC combination, and between 2.07% and 16.77%, for the

Table 4
Hybrid composites tested under fatigue loading.

No.	Specimen	F_{max} [kN]		σ_{max} [MPa]	N_f
		Nominal	Actual		
1	GC-F-100-415	10.00	10.24	295.7	4900
2	GC-F-100-416	10.00	10.36	288.1	25,900
3	GC-F-100-720	10.00	10.22	294.1	17,400
4	GC-F-100-721	10.00	10.24	281.0	34,000
5	GC-F-120-411	12.00	12.22	353.0	3400
6	GC-F-120-412	12.00	12.25	355.2	4600
7	GC-F-120-414	12.00	12.26	344.4	1900
8	GC-F-135-110	13.50	13.81	388.6	1009
9	GC-F-135-111	13.50	13.79	375.8	669
10	GC-F-135-112	13.50	13.76	398.9	1400
11	GC-F-150-710	15.00	15.33	431.1	574
12	GC-F-150-814	15.00	15.29	451.3	232
13	GC-F-165-810	16.50	16.82	510.9	409
14	GC-F-165-813	16.50	16.80	498.1	309
15	GC-F-165-816	16.50	16.77	508.0	209

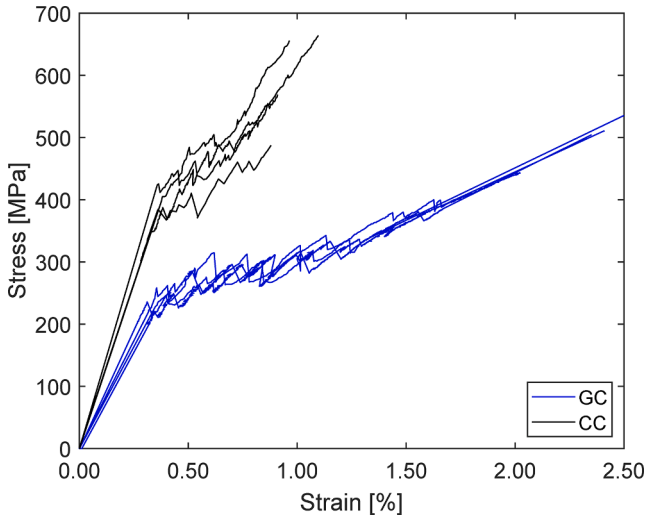

Fig. 4. Pseudo-ductile tensile responses of GC and CC combinations.

Table 5
Tensile properties obtained in quasi-static tests.

Specimen	Elastic modulus [GPa]	σ@LF [MPa]	Strain at the failure of LS fibers [%]	Tensile strength [MPa]	Strain at the failure [%]	ε_{pd} [%]
GC-QS-01	77.8	234.9	0.30	443.6	2.01	1.44
GC-QS-02	65.6	220.2	0.33	504.4	2.33	1.56
GC-QS-03	69.2	234.9	0.34	510.8	2.40	1.66
GC-QS-04	69.2	258.2	0.35	535.8	2.49	1.71
Mean (COV [%])	70.5 (7.4)	237.1 (6.6)	0.33 (6.61)	498.6 (7.9)	2.31 (9.06)	1.59 (7.64)
CC-QS-01	110.2	384.6	0.36	487.4	0.88	0.44
CC-QS-02	108.2	351.6	0.33	569.1	0.91	0.38
CC-QS-03	106.5	406.5	0.41	655.8	1.00	0.39
CC-QS-04	111.7	430.3	0.39	663.8	1.13	0.54
Mean (COV [%])	109.2 (2.1)	393.3 (8.5)	0.37 (8.89)	594.0 (14.0)	0.98 (11.69)	0.44 (16.77)

analyzed properties of CC combination.

The elastic modulus, according to ISO 527–5 [41], was defined as the slope of stress–strain curve for the strains 0.0005 and 0.0025. A mean value of 70.5 GPa (COV = 7.4%) was obtained for the case of GC combination, while for CC combination was equal to 109.2 GPa (COV = 2.1%).

In the case of GC combination, a mean 'yield' stress of 237.1 MPa and a mean pseudo-ductile strain of 1.59% were registered. In CC combination a mean 'yield' stress of 393.3 MPa and a mean pseudo-ductile strain of 0.44% were registered. The CHM ply started to fragment when the strain reached ca. 0.3–0.4%. This value is higher than the strain at failure of a single CHM composite layer, measured as 0.27% in [21]). In this case the hybrid effect of ca. 30% can be largely attributed to changes of stress concentrations and stress recovery at a broken fiber due to the presence of neighboring fibers with different stiffness. The substantial increase in strain of the LS fibers is caused by the restraint from the adjacent HS fibers, which inhibits the formation of broken clusters of LS material.

The strain at the failure of LS fibers (first crack) are identical in both combinations. The *t* statistical test (*t*-test) was used to assess if these mean values are statistically different from each other. The *p*-value was obtained. The *p*-value is the smallest level of significance that would lead to rejection of the null hypothesis and varies between 0 and 1. In the present case, the null hypothesis is that the mean strain at the failure of LS fibers is equal in both cases. The level of significance is the probability of rejecting the null hypothesis when it is true. The computed *p*-values was 0.084. Since *p*-value is higher than 0.050, it can be stated that the null hypothesis cannot be rejected, and therefore hybrid combination did not promote differences in mean strain at the failure of LS fibers.

As explained in Czel et al. [23], stable pull out of LS layer is only possible if, after it fracture, the rest of the laminate is able to withstand the applied load. For this to occur, the strain energy release rate (G_r) should be lower than the delamination toughness (G_{IIC}). G_r can be approximately estimated for the GC and CC combinations by the following equation:

$$G_r = \frac{\sigma_{LS}^2 t_{LS}(E_{HS}(h - t_{LS}) + E_{LS}t_{LS})}{4E_{HS}E_{LS}(h - t_{LS})} \quad (1)$$

where *h* is the specimen's nominal thickness, and *E* and *t* are the stiffness and the nominal cured layer thickness, while the subscripts LS and HS refer to the low strain and high strain layers, respectively.

The stress at the LS layer can be computed by equation (2):

$$\sigma_{LS} = \frac{\sigma h E_{LS}}{4E_{HS}E_{LS}(h - t_{LS})} \quad (2)$$

The stiffness of the CHM, CLM, and G were considered to be 113.64 GPa, 61.90 GPa, and 20.09 GPa, according to previous characterization of these materials performed by the authors' group in [22]. Considering the proportion of the CHM layer in the total of layers of each combination, it was assumed that t_{LS} is equal to 0.545 mm and 0.597 mm for the combination GC and CC, respectively. The computed G_r values were 1.346 N/mm and 0.781 N/mm for GC and CC, respectively, being lower than the previously estimated G_{IIC} (1.46 N/mm for GC and 1.25 N/mm for CC in [22]).

Fig. 5 shows the typical failure for both GC and CC specimens under quasi-static loading. In Fig. 5(a), it is possible observe delamination areas at the specimen because the outside layers of the tested specimen are translucent (glass/epoxy). In this case, the well bonded area is black, due to the natural CHM color. During the test, CHM cracks were followed by stable delamination between layers. Delamination areas appeared in a distributed manner along the gauge length forming a striped pattern. The delamination areas developed stably during loading until almost linking up. After that, the final failure occurred at glass/epoxy layers. In Fig. 5(b) only the final failure of standard modulus carbon/epoxy (outside layers) is visible. In this case, the variation of the longitudinal strains was measured by a 2D DIC system. Fig. 6 shows the stress–strain curve for specimen CC-QS-03 and the observed surface strain fields obtained with the 2D DIC system (consecutive phases of tensile test of specimen). The colored scale corresponds to the measured strains. The observation of the strain fields allowed to establish the relationship between the cracking of CHM, propagation of delamination and the stress–strain curve. The 2D DIC system allowed to observe the fragmentation of CHM and localized delamination between layers (identified by high values of the longitudinal strain). It was observed that delamination has been developed steadily during loading until the specimen saturation. This is an important output, since in the case of CC

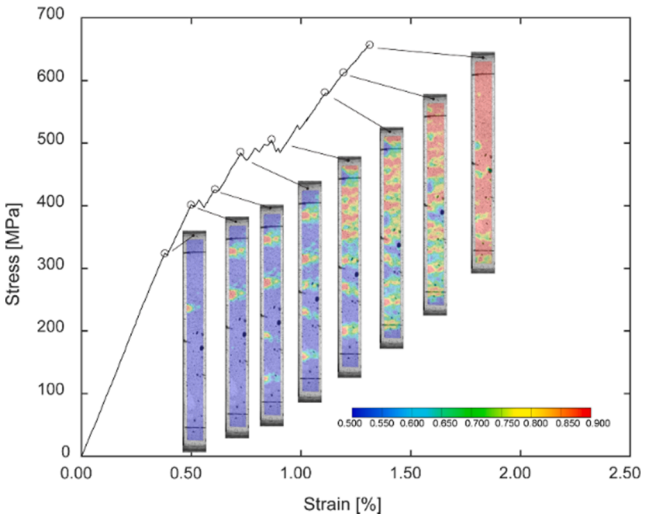

Fig. 6. Strain field of CC combination (CC-QS-03 specimen) during loading.

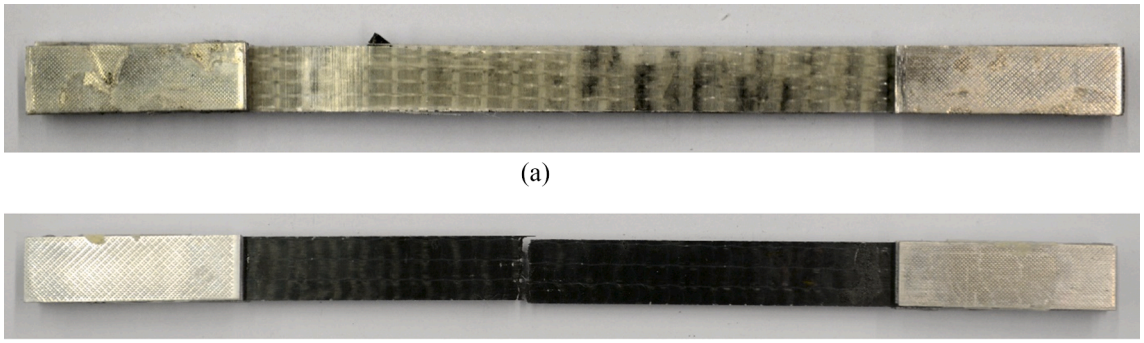

(a)

(b)

Fig. 5. Failure modes: (a) GC and (b) CC combinations.

combination fragmentation and delamination cannot be noted visually.

4.2. Low-cycle experiments

Low-cycle quasi-static experiments were performed in order to investigate the influence of the cyclic loading on the stiffness variation and residual strain of hybrid combinations. Typical low-cycle stress–-strain curves are shown in Fig. 7. From these curves, it is possible to observe the stiffness degradation and the residual (plastic) strain during the cyclic phase. As it was referred to, specimens have been always subjected to a minimum tensile force of 0.5 kN. After reaching the maximum stress in each cycle, the specimen was unloaded to the minimum load. At this point, the residual strain was measured.

Fig. 8 shows the residual strain as function of the ratio between the maximum stress of cycle and the tensile strength (σ_N/σ_{ult}). For both combinations, it is possible to observe that a very small residual strain was registered. This is in agreement with Wisnom *et al.* [43] that also concluded that carbon/glass hybrid composites have very small (<0.2%) residual strain. In the case of CC combination, the residual strain was always below 0.1%. For both combinations, it is possible to observe that until $\sigma_N/\sigma_{ult} = 0.5$ residual strains are almost zero, this correspond to the initial elastic phase of the stress strain material behavior, presented in Fig. 4. After that, there is an increase of residual strains, during the fragmentation phase. Finally, during the final phase, the behavior of the specimens is dominated by the elastic properties of the HS materials. At this phase, residual strains are almost constant, in GC combination that presents a long, almost, linear final stage at the stress–strain diagram. In the case of CC combination, since the final linear stage at the stress–strain diagram is very short (see Fig. 4), it was not possible to observe the constant strain stage in Fig. 8(b).

Stiffness degradation of all tested specimens is shown in Fig. 9. As expected, stiffness degradation begins after strain at failure of CHM is reached. Damage in the hybrids consists primarily of layer fragmentation and localized delamination, and this does lead to a loss in modulus as the fragmenting layer gradually contributes less and less to the overall stiffness of the laminate. It could be observed that before strain at failure of CHM there are small variations of stiffness. This is due to the fact the start of the stress–strain curve has more influence in determining the initial stiffness of elasticity, since less points are considered to determine the stiffness. Besides, there is a small variation of initial stiffness comparatively to elastic modulus obtained at quasi-static tests. This is due to the fact that the elastic modulus, according to ISO 527–5 [41], is defined as the slope of the fitted line to the stress–strain curve for the strains 0.0005 and 0.0025 while the stiffness at cyclic tests was computed through linear regression, taking into account all the points of a cyclic (unloading/reloading components). For both cases, the stiffness is limited by the undamaged hybrid material (upper bound) and by a "theoretical" specimen without the contribution of the LS material (lower bound). The stiffness of CLM and G were considered 61.90 and 20.09 GPa [22], respectively.

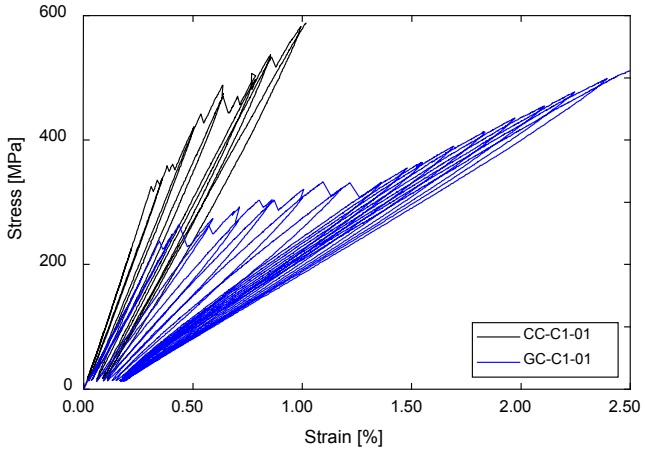

Fig. 7. Low-cyclic test response and corresponding stiffness degradation.

Table 6 summarizes the main mechanical properties obtained from the low-cycle experiments. Comparison of Tables 5 and 6 shows that very similar tensile properties were obtained from quasi-static and from low-cycle experiments, although a higher dispersion was observed for the results obtained from the low-cycle experiments. This observation may indicate that the loading type can influence the results dispersion. The highest dispersion was registered at the failure strain and at the pseudo-ductile strain, i.e., in the properties of materials at failure. However, considering the small number of tests carried out, this subject should be further investigated. In the case of GC combination, a mean 'yield' stress of 247.1 MPa and a mean pseudo-ductile strain of 1.70% were registered. In CC combination a mean 'yield' stress of 366.3 MPa and a mean pseudo-ductile strain of 0.36% were registered. The highest strength was achieved with CC combination. Similarly to that was observed at quasi-static results, the main strain at the failure of LS fibers are identical in both combinations. This was expected, since LS material (CHM) is the same at both combinations. The highest 'yield' stress and elastic modulus were achieved with CC combination. Again, the highest pseudo-ductile strain was achieved with GC combination.

The *t*-test was used to assess whether the mean values of the quasi-static and the low-cycle experiments are statistically different from each other. In the present case, the null hypothesis is that the mean mechanical properties that comes from quasi-static tests equals the mean mechanical properties that comes from low-cycle tests. The computed *p*-values for elastic modulus, σ@LF, strain at the failure of LS fibers, tensile strength, strain at the failure, and ε_{pd} were 0.862, 0.254, 0.387, 0.256, 0.361, 0.228, respectively for GC combinations and 0.130, 0.316, 0.145, 0.401, 0.435, and 0.387, respectively for CC combinations. Given the large computed *p*-values (above 0.05), it can be stated that the null hypothesis cannot be rejected, i.e., quasi-static and low-cycle tests lead to identical mechanical results, although the dispersion of results influences the previous statement.

4.3. Fatigue experiments

The fatigue life of the examined specimens varied between 209 and 34,000 cycles (see Table 4) – these are relatively low cycle numbers when compared with the preliminary results of CC combinations. It was observed that fatigue life of specimens was limited by the failure of the glass fibers. As expected, during fatigue loading the temperature of the specimens increased due to the self-generated heating as a result of internal friction. At low stress levels, a maximum temperature of ca. 40 °C was measured locally, while for higher stress levels the local maximum temperature was less reaching ca. 25 °C due to the lower number of fatigue cycles until failure. According to the DMA results, the temperatures were well below the *Tg* onset and inside the limits of the epoxy glassy region.

The fatigue failure data are presented in the S-N curve diagram shown in Fig. 10. As mentioned in a number of documents, e.g. [29,44] several types of formulations can be used for simulating the fatigue experimental results. Nevertheless, in this work the simple power law formulation, shown in Eq. (3) was applied by using the *CCfatigue* software [45].

$$\sigma_{max} = \sigma_o N^{-\frac{1}{k}} \tag{3}$$

with σ_o, $1/k$ been the model parameters derived by linear regression analysis, after fitting Eq. (1) to the available experimental fatigue data, which are 1012.85 and 0.132, respectively.

As it is known [38,39], for materials with a purely elastic behavior, the elastic energy per cycle is equal to the total energy and no dissipation energy is measured. However, for the majority of materials, energy is

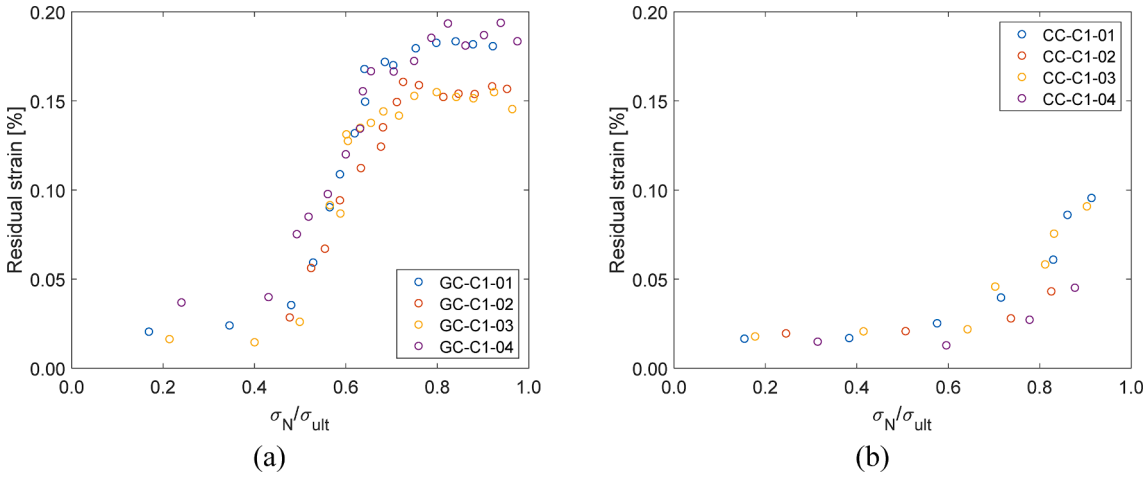

Fig. 8. Residual strain at different loading point for all tested specimens: a) GC and (b) CC combinations.

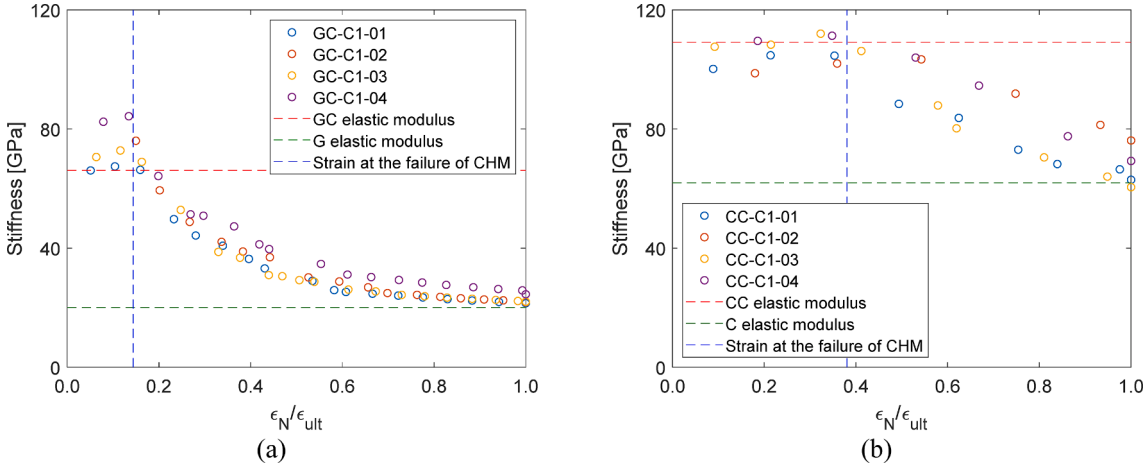

Fig. 9. Stiffness degradation of all tested specimens: a) GC and (b) CC combinations.

Table 6
Tensile properties obtained in low-cycle tests.

Specimen	Elastic modulus [GPa]	σ@LF [MPa]	Strain at the failure of LS fibers [%]	Tensile strength [MPa]	Strain at the failure [%]	ε_{pd} [%]
GC-C1-01	66.1	237.7	0.35	518.22	2.54	1.76
GC- C1-02	66.1	249.3	0.32	527.31	2.48	1.68
GC- C1-03	70.6	251.1	0.34	535.25	2.53	1.77
GC- C1-04	82.4	253.6	0.41	514.72	2.20	1.57
Mean (COV [%])	71.3 (10.8)	247.9 (2.9)	0.35 (11.24)	523.88 (1.77)	2.44 (6.65)	1.70 (5.51)
CC-C1-01	100.2	322.7	0.31	588.78	1.02	0.43
CC-C1-02	98.8	351.0	0.34	503.77	0.70	0.19
CC-C1-03	107.6	398.2	0.36	594.29	1.06	0.51
CC-C1-04	109.6	393.4	0.35	516.52	0.79	0.32
Mean (COV [%])	104.1 (5.2)	366.3 (9.8)	0.34 (6.92)	550.84 (8.59)	0.89 (19.63)	0.36 (38.36)

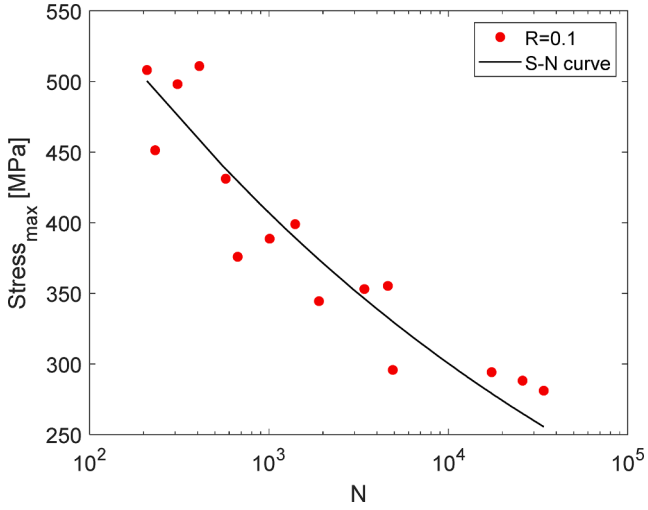

Fig. 10. Experimental fatigue data and S-N curve of GC combination.

dissipated at each loading cycle, either due to additional structural changes, or due to hysteretic heating.

During a load-controlled fatigue experiment, the hysteresis loops can shift, indicating the presence of creep and the evolution of the average

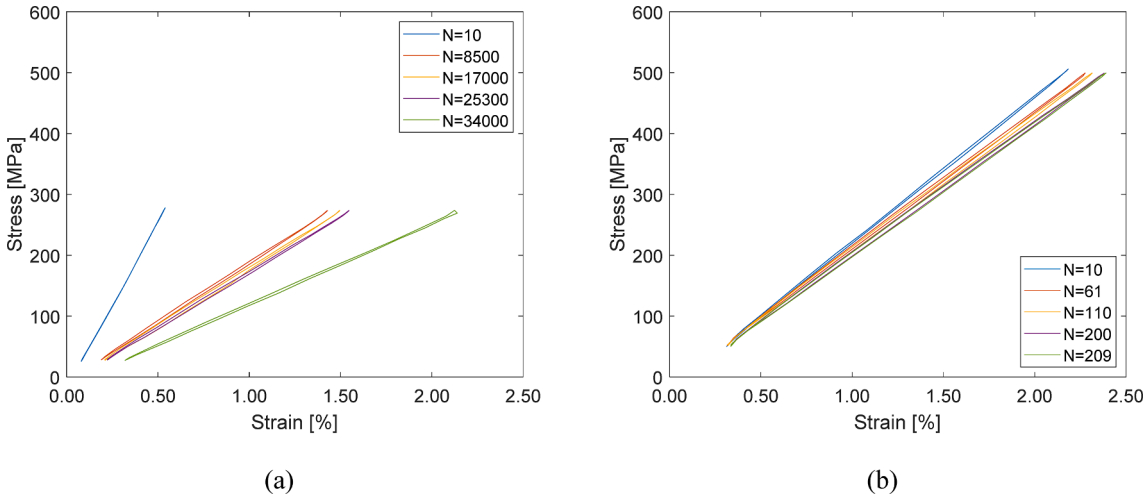

Fig. 11. Hysteresis loops variation with cycle for GC hybrids (a) GC-F-100-720, (b) GC-F-165-816.

strain per cycle can be monitored to describe creep behavior [31]. Typical hysteresis loops up to failure are presented in Fig. 11 for low (281 MPa) and high (508 MPa) maximum stress levels. Although only selected results are presented, they are representative of the behavior exhibited by all other specimens. For all specimen series and at all stress levels, the material response shown elastic stress–strain hysteresis loops with little hysteresis area. Small stiffness changes were observed at higher stress level, but significant changes between first cycles and the remaining cycles were observed at tests performed at lower stress levels.

In Fig. 12, the normalized fatigue stiffness, E_N, with respect to the stiffness of the first cycle, E_1, is plotted against the normalized fatigue life. One representative example of each load level is presented, showing a consistent trend with less stiffness degradation for higher stress levels and more stiffness degradation for lower stress levels, in agreement with observations in other works for non-hybrid composites, e.g., [32,46]. Nevertheless, stiffness degradation, irrespective of stress level, followed the same pattern. An initial steep decrease until 20% of the lifetime was followed by a steady state decreasing trend up to the failure of all specimens. It was observed that as cyclic stresses decreased, fatigue stiffness and failure stiffness decreased further, i.e., more damage was accumulated during the loading, for longer lifetimes, as explained in details in [32] for non-hybrid angle-layer composite laminates.

The slope of the steady state segment was steeper for higher stress levels. However, the initial stiffness drop was more pronounced for those specimens loaded at lower stress levels. In this case, the low load level led to a limited number of cracks at the carbon layer (2 or 3 cracks) during the first loading cycles, followed by propagation of delamination between the carbon and glass layers. The fatigue damage progress and the corresponding stiffness degradation are shown in Fig. 13. The supplementary video related to the described behavior of the specimen can be found in Appendix A. Until complete delamination the decrease of stiffness was more evident than in the remaining lifetime (see Fig. 13). In the case of higher load levels, more cracks appear, already during the first loading, before the application of the fatigue cycles. Therefore, a significant stiffness reduction during fatigue is not expected since the specimen has already a reduced stiffness.

The average cyclic strain *versus* the normalized number of cycles is shown in Fig. 14. This strain is attributed to creep in elastic/viscoelastic materials and it is expected to increase with loading under stress controlled experiments. As shown in Fig. 14, most of the specimens (especially those at the higher stress levels) do not show any considerable increase of the average cyclic strain, while only the specimens loaded at the lowest stress levels showed a small increase during the first stages of the loading. At higher stress levels, the specimens delaminated at the first monotonic loading and therefore, no significant strain increase was monitoring during the rest of the fatigue loading. In contrast

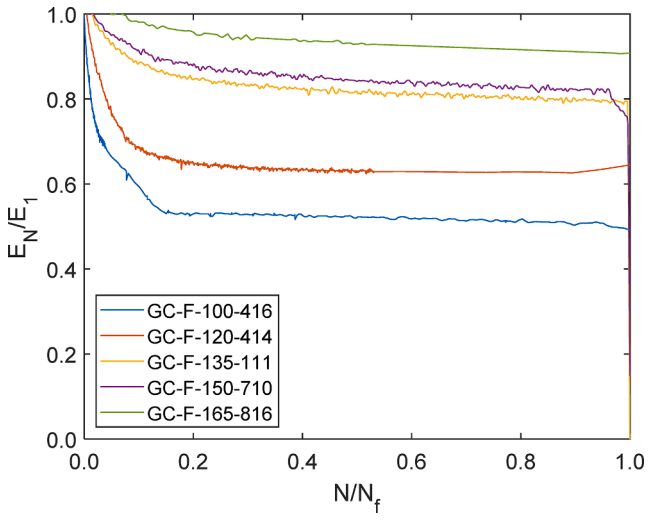

Fig. 12. Normalized fatigue stiffness vs. normalized number of cycles at different stress levels.

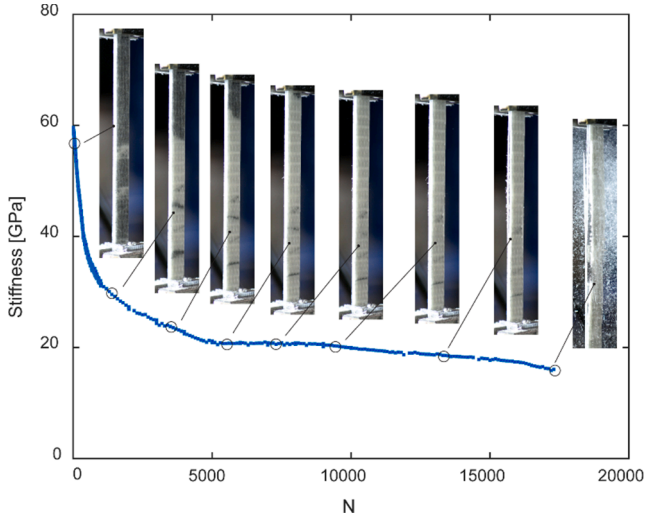

Fig. 13. Damage and stiffness degradation during the fatigue test at lowest maximum stress level.

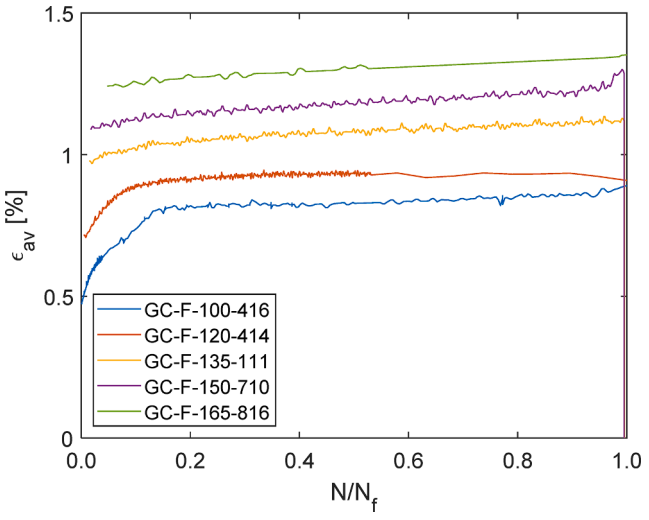

Fig. 14. Average cyclic strain *versus* normalized number of cycles at different load levels.

to that, at lower cyclic stress levels, delamination initiated and propagated later on, during the fatigue experiments, resulting in the observed average cyclic strain increase, as shown in Fig. 14. In contrast to other observations for elastic/viscoelastic materials, e.g., [24–26] this increase is not attributed to creep but is rather a result of the damage accumulation due to the delamination.

Since a complete delamination occurs during fatigue loading, the LS material has a reduced contribution in the observed behavior after that. The pseudo-ductility is not explored during fatigue loading since no more cracks at LS material occur during the test. However, before delamination, in the case of lower load levels, there is a benefit in terms of stiffness of hybrid specimens compared to specimens entirely made of HS material.

5. Conclusions

The experimental behavior of glass/ultra high modulus carbon (GC) and high strength carbon/ultra high modulus carbon (CC), pseudo-ductile, UD hybrid composite laminates, under quasi-static low-cyclic loading, and fatigue loading was investigated in this paper. The CC laminated were proved very resistant to fatigue loading, reaching or exceeding $5x10^6$ fatigue cycles for maximum cyclic stresses approaching the yield stress level. Therefore, the fatigue behavior investigation was mainly focused on the analysis of the GC laminates.

The following conclusions can be drawn from this work:

- DIC allowed to observe fragmentation and delamination propagation in both material systems, allowing the damage progression monitoring in the CC laminates, where, due the opaque materials, any damage cannot be observed by visual inspection.
- Pseudo-ductile tensile response with multiple fractures was observed under quasi-static loading. The CC laminates exhibited higher initial elastic modulus, 'yield' stress and strength while the GC laminates showed the highest pseudo-ductile strain.
- The elastic modulus, the strain at failure of the LS fibers, the tensile strength, and the strain at failure were affected by the low cycle loading; a small amount of residual (plastic) deformation was observed.
- The fatigue behavior of the GC laminates can be simulated by commonly used power law formulations as non-hybrid composite materials. Little hysteresis area was observed during the fatigue testing at all stress levels. The fatigue stiffness variation with fatigue cycles was minimal at high stress levels, but pronounced for low stress levels when more distributed damage was accumulated in the specimen volume.
- Significant damage was accumulated to the specimens during loading and the last phase, leading to failure that occurred after the delamination between the glass and carbon layers.

Declaration of Competing Interest

The authors declare that they have no known competing financial interests or personal relationships that could have appeared to influence the work reported in this paper.

Acknowledgements

The authors acknowledge the assistance provided by the technical team of the structural engineering Experimental platform (GIS-ENAC at the Ecole Polytechnique Fédérale de Lausanne (EPFL), Switzerland) for the use of testing equipment, and the support of S&P Clever Reinforcement, that provided the raw materials (E-glass, standard and high modulus carbon sheets and the epoxy adhesive). The first author acknowledge the STSM grant provided by COST Action CA18120 (CERTBOND), supported by COST (European Cooperation in Science and Technology). The second author acknowledge his sabbatical grant SFRH/BSAB/150266/2019, provided by Fundação para a Ciência e a Tecnologia, IP (FCT), financed by European Social Fund and by national funds through the FCT/MCTES and also the financial support by the EPFL/Section of Civil engineering. This work is also part of the research project 'EasyFloor – Development of composite sandwich panels for rehabilitation of floor buildings', involving the company ALTO – Perfis Pultrudidos, Lda., CERis/Instituto Superior Técnico and ISISE/University of Minho, supported by FEDER funds through the Operational Program for Operational Program for Competitiveness and Internationalization (POCI) and the Portuguese National Innovation Agency (ANI) – Project No. 3480 (POCI-01-0247-FEDER-003480).

Appendix A. Supplementary material

Supplementary data to this article can be found online at https://doi.org/10.1016/j.ijfatigue.2021.106143.

References

[1] Fernando G, Dickson RF, Adam T, Reiter H, Harris B. Fatigue behaviour of hybrid composites - Part 1 Carbon/Kevlar hybrids. J Mater Sci 1988;23(10):3732–43.
[2] Vassilopoulos AP. The history of fiber-reinforced polymer composite laminate fatigue. Int J Fatigue 2020;134:105512.
[3] Swolfs Y, Gorbatikh L, Verpoest I. Fibre hybridisation in polymer composites: a review. Compos A Appl Sci Manuf 2014;67:181–200.
[4] Summerscales J, Short D. Carbon fibre and glass fibre hybrid reinforced plastics. Composites 1978;9:157–66.
[5] Wu Z, Shao Y, Iwashita K, Sakamoto K. Strengthening of preloaded RC beams using hybrid carbon sheets. J. Compos. Constr. 2007;11:299–307.
[6] Swolfs Y. Perspective for fibre-hybrid composites in wind energy applications. Materials 2017;10(11):1281.
[7] Hofer K, Bennett L, Stander M. Effects of moisture and fatigue on the residual mechanical properties of S-glass/graphite/epoxy hybrid composites. In: Fatigue of filamentary composite materials. ASTM International; 1977.
[8] Pegoretti A, Fabbri E, Migliaresi C, Pilati F. Intraply and interply hybrid composites based on E-glass and poly (vinyl alcohol) woven fabrics: tensile and impact properties. Polym Int 2004;53:1290–7.
[9] Hofer Jr K, Stander M, Bennett L. Degradation and enhancement of the fatigue behavior of glass/graphite/epoxy hybrid composites after accelerated aging. Polym Eng Sci 1978;18:120–7.
[10] Phillips LN. Improving racing-car bodies. Composites 1969;1:50–1.
[11] Marron G, Fisher S, Tuler FR, Wagner HD. Hybrid effects in composites: conditions for positive or negative effects versus rule-of-mixtures behaviour. J Mater Sci 1978;13:1419–26.
[12] Hayashi I, Asanuma K-I, Niwa K, Fukano M, Maruyama N. Mechanism of damage propagation in CFRP/AFRP hybrid laminates under fatigue flexural loading. JSME Int J Ser 1, Solid Mech Strength Mater 1991;34:240–8.
[13] Harel H, Aronhime J, Schulte K, Friedrich K, Marom G. Rate-dependent fatigue of aramid-fibre/carbon-fibre hybrids. J Mater Sci 1990;25:1313–7.

[14] Abd El-Baky M, Attia M. Flexural fatigue performance of hybrid composite laminates based on E-glass and polypropylene fibers. J Thermoplast Compos Mater 2019;32:228–47.
[15] Peijs A, De Kok J. Hybrid composites based on polyethylene and carbon fibres. Part 6: Tensile and fatigue behaviour. Composites 1993;24:19–32.
[16] Wu Z, Wang X, Iwashita K, Sasaki T, Hamaguchi Y. Tensile fatigue behaviour of FRP and hybrid FRP sheets. Compos B Eng 2010;41:396–402.
[17] Selmy A, El-baky MA, Azab N. Experimental study on flexural fatigue behavior of glass fibers/epoxy hybrid composites with statistical analysis. J Reinf Plast Compos 2013;32:1821–34.
[18] Sharba MJ, Leman Z, Sultan MT, Ishak MR, Hanim MAA. Effects of kenaf fiber orientation on mechanical properties and fatigue life of glass/kenaf hybrid composites. BioResources 2016;11:1448–65.
[19] Sivakumar D, Ng L, Lau S, Lim K. Fatigue life behaviour of glass/kenaf woven-ply polymer hybrid biocomposites. J Polym Environ 2018;26:499–507.
[20] Mostafa NH. Tensile and fatigue properties of Jute-Glass hybrid fibre reinforced epoxy composites. Mater Res Express 2019;6:085102.
[21] Shahzad A. Impact and fatigue properties of hemp–glass fiber hybrid biocomposites. J Reinf Plast Compos 2011;30:1389–98.
[22] Ribeiro F, Sena-Cruz J, Branco FG, Júlio E. Hybrid effect and pseudo-ductile behaviour of unidirectional interlayer hybrid FRP composites for civil engineering applications. Constr Build Mater 2018;171:871–90.
[23] Czél G, Wisnom MR. Demonstration of pseudo-ductility in high performance glass/epoxy composites by hybridisation with thin-ply carbon prepreg. Compos A Appl Sci Manuf 2013;52:23–30.
[24] Sharba M, Leman Z, Sultan M, Ishak M, Hanim M. Monotonic and fatigue properties of kenaf/glass hybrid composites under fully reversed cyclic loading. In: 3rd Int, Conf. Mech. Eng. Res.(ICMER 2015), IOP Publishing IOP Conf. Series: Materials Science and Engineering; 2015.
[25] Dickson R, Fernando G, Adam T, Reiter H, Harris B. Fatigue behaviour of hybrid composites. J Mater Sci 1989;24:227–33.
[26] Dai G, Mishnaevsky Jr L. Fatigue of hybrid glass/carbon composites: 3D computational studies. Compos Sci Technol 2014;94:71–9.
[27] Philippidis TP, Vassilopoulos A. Fatigue design allowables for GRP laminates based on stiffness degradation measurements. Compos Sci Technol 2000;60:2819–28.
[28] Zhang Y, Vassilopoulos AP, Keller T. Fracture of adhesively-bonded pultruded GFRP joints under constant amplitude fatigue loading. Int J Fatigue 2010;32:979–87.
[29] Sarfaraz R, Vassilopoulos AP, Keller T. Experimental investigation of the fatigue behavior of adhesively-bonded pultruded GFRP joints under different load ratios. Int J Fatigue 2011;33:1451–60.
[30] Savvilotidou M, Keller T, Vassilopoulos AP. Fatigue performance of a cold-curing structural epoxy adhesive subjected to moist environments. Int J Fatigue 2017;103:405–14.
[31] Foletti AI, Cruz JS, Vassilopoulos AP. Fabrication and curing conditions effects on the fatigue behavior of a structural adhesive. Int J Fatigue 2020;139:105743.
[32] Movahedi-Rad AV, Keller T, Vassilopoulos AP. Fatigue damage in angle-ply GFRP laminates under tension-tension fatigue. Int J Fatigue 2018;109:60–9.
[33] Suwarta P, Fotouhi M, Czél G, Longana M, Wisnom MR. Fatigue behaviour of pseudo-ductile unidirectional thin-ply carbon/epoxy-glass/epoxy hybrid composites. Compos Struct 2019;224:110996.
[34] Ribeiro F, Sena-Cruz J, Branco FG, Júlio E. Hybrid FRP jacketing for enhanced confinement of circular concrete columns in compression. Constr Build Mater 2018;184:681–704.
[35] Ribeiro F, Sena-Cruz J, Branco FG, Júlio E. 3D finite element model for hybrid FRP-confined concrete in compression using modified CDPM. Eng Struct 2019;190:459–79.
[36] Ribeiro F, Sena-Cruz J, Branco FG, Júlio E, Castro F. Analytical hybrid effect prediction and evolution of the tensile response of unidirectional hybrid FRP composites for civil engineering applications. J Compos Mater 2020.0021998320911956.
[37] Jalalvand M, Czél G, Wisnom MR. Parametric study of failure mechanisms and optimal configurations of pseudo-ductile thin-ply UD hybrid composites. Compos A 2015;74:123–31.
[38] Jalalvand M, Czél G, Wisnom MR. Damage analysis of pseudo-ductile thin-ply UD hybrid composites – A new analytical method. Compos A 2015;69:83–93.
[39] Namourah Z. Exploring the use of hybrid FRP composites on retrofitting of RC beam-column joints. Msc Dissertation. University of Minho; 2019.
[40] ISO. 527-2 Plastics — Determination of tensile properties — Part 2: Test conditions for moulding and extrusion plastics. European Committee for Standardization; 2012.
[41] ISO. 527-5 Plastics — Determination of tensile properties; Part 5: Test conditions for unidirectional fibre-reinforced plastic composites. European Committee for Standardization; 2009.
[42] Hollaway LC, Leeming MB. Strengthening of reinforced concrete structures. using externally-bonded FRP composites in structural and civil engineering. Woodhead Publishing Limited Cambridge England; 1999.
[43] Wisnom MR, Fuller JD, Suwarta P, Czel G. Repeated Tensile loading of thin-ply pseudo-ductile laminates. In: Proceedings of the American Society for Composites - 30th Technical Conference, ACS 2015 American Society for Composites; 2015.
[44] Sarfaraz R, Vassilopoulos AP, Keller T. Modeling the constant amplitude fatigue behavior of adhesively bonded pultruded GFRP joints. J Adhes Sci Technol 2013;27(8):855–78.
[45] Vassilopoulos AP, Sarfaraz R, Manshadi BD, Keller T. A computational tool for the life prediction of GFRP laminates under irregular complex stress states: influence of the fatigue failure criterion. Comput Mater Sci 2010;49(3):483–91.
[46] Movahedi-Rad AV, Keller T, Vassilopoulos AP. Interrupted tension-tension fatigue behavior of angle-ply GFRP composite laminates. Int J Fatigue 2018;113:377–88.